Title

Simulating Nonlinear Optical Pulse Shaping to Optimize LCLS Photoinjector and XFEL Operation at SLAC

Authors

McKeown-Green, Amy
Hirschman, Jack
Carbajo, Sergio

Publication Date

2021-07-01

Simulating Nonlinear Optical Pulse Shaping to Optimize LCLS Photoinjector and XFEL Operation at SLAC

A.McKeown-Green,[1] J.Hirschman,[2] and S.Carbajo[2]
[1)] *SULI intern, U.S. Department of Energy, Office of Science, Office of Workforce Development for Teachers and Scientists.*
[2)] *SLAC National Accelerator Laboratory and Stanford University, 2575 Sand Hill Rd, Menlo Park, CA 94025, USA*

(Dated: 20 August 2021)

ABSTRACT

X-ray free-electron lasers (XFEL) allow for the investigation of physical and chemical phenomena at the femtosecond timescale. XFEL x-ray pulses are generated via the undulation of near-relativistic electron bunches and inherit much of the bunches' phase and temporal shaping. The peak energy and time duration of XFEL x-ray pulses can thus be improved by controlling the initial shaping of the electron bunches by the photoinjector system. To this end, a multistep simulation of photoinjector laser pulse generation and shaping is being developed. One key step in this simulation is the expansion of a computer program which models sum frequency generation in a nonlinear crystal for up-conversion to the UV via the interaction of two chirped infrared pulses. In this work, the program was modified to allow for the input of more exotic pulses previously shaped using an acousto-optic programmable dispersive filter (AOPDF) simulator. The simulated output pulses were then formatted for use in the next step of the multi-process simulation.

I. INTRODUCTION

The Linac Coherent Light Source (LCLS) at SLAC National Laboratory is a 3 km-long x-ray free-electron laser (XFEL) which produces high energy, ultrafast x-ray pulses.[1] To improve the peak x-ray energy of these pulses and thus enable the investigation of novel physical phenomenon, we seek to optimize pulse generation through the application of machine learning techniques to a comprehensive simulation of the LCLS XFEL. The photoinjector stage of the simulation is currently being developed and models the process by which a shaped UV pulse is generated and held incident on a copper photocathode to produce electron bunches. Though not currently under development, additional stages in the simulation will be created to model the acceleration of these generated electron bunches to near-relativistic speeds and their undulation to produce ultrafast, high energy x-ray pulses.

The laser-centered component of the photoinjector simulation describes the shaping and up-conversion of IR light to the UV and was the focus of this work. A parent pulse is first generated using a simulated carbide laser, yielding a gaussian temporal pulse with a central wavelength of 1030 nm and a pulse width of approximately 330 fs. The pulse then undergoes both amplitude and phase shaping by an acousto-optic programmable dispersive filter (AOPDF) simulator. The newly shaped pulse continues on, entering a regenerative amplifier which reduces bandwidth while increasing pulse intensity. Next, the parent pulse is split into two pulses and each child pulse is stretched/compressed to yield two broadly dispersed pulses. Finally, the two pulses enter the sum frequency generation (SFG) simulation where they undergo noncolinear mixing to produce a highly tunable pulse with a central wavelength of 515 nm. The output pulse then undergoes a further up-conversion step to bring it into the UV. Previous literature details the development of an original SFG simulation computer program which modeled both the stretching/compressing of the two split pulses and their mixing in a nonlinear crystal.[2] This report details the expansion of this original program and its integration into the broader photoinjector system simulation, including a demonstration of the processing of exotically shaped parent pulses.

However, before a detailed discussion of these program modifications can occur, it is necessary to summarize the underlying principles of pulse dispersion and SFG. The pulses used in the simulation were defined by an electric field with a characteristic amplitude and phase (Eq. 1).

$$E(\omega) = A(\omega)e^{i\phi(\omega)} \tag{1}$$

This phase can be represented as a Taylor expansion with 1st, 2nd, and 3rd order Taylor coefficients corresponding to the 1st, 2nd, and 3rd order phase term of the pulse (Eq.2).

$$\phi(\omega) = \phi_1 + \frac{\phi_2}{2!}(\omega-\omega_o)^2 + \frac{\phi_3}{3!}(\omega-\omega_o)^3 + \frac{\phi_4}{4!}(\omega-\omega_o)^4 + ... \tag{2}$$

Consequently, the stretching/compressing of the split input pulses in the original program corresponds to multiplying the input pulses by an exponential phase term containing non-zero 2nd and 3rd order Taylor coefficients.

Following the addition of 2nd and 3rd order phase, the two dispersed pulses then enter the SFG simulation where they interact with a nonlinear medium. Nonlinear optical properties occur when a material's response is not directly proportional to the incident electric field.[3] One key example of a nonlinear optical process is SFG where two input beams, with respective frequencies ω_1 and ω_2, mix to generate a third beam with a frequency $\omega_3 = \omega_1 + \omega_2$ as can be seen in Fig. 1a.[3] SFG can also be modeled as two photons, with respective frequencies ω_1 and ω_2, exciting the system to a higher energy virtual state. When the system transitions to the ground state, a single photon with frequency $\omega_3 = \omega_1 + \omega_2$ is emitted (Fig. 1b).

The behavior of the three electric fields corresponding to ω_1, ω_2, and ω_3 is governed by the nonlinear Maxwell equations.[3] Consequently, the amplitudes of the three electric fields A_1, A_2, and A_3 can be described by the series of coupled differential equations given in Eqs. 3a ,b, and c.[3]

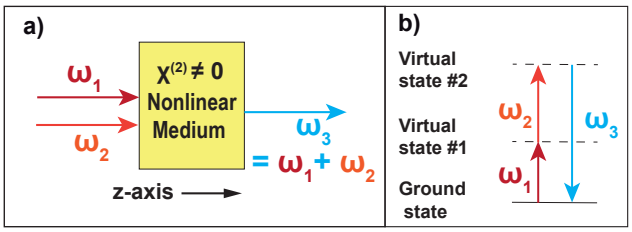

FIG. 1. a) Diagram showing the mixing of two input electric fields (orange and red) to generate a third field (blue) in SFG. b) Virtual state diagram for the SFG.

$$\frac{dA_1}{dz} = d_{eff} i \frac{2k_1}{n_o(\lambda_1)} A_2^* A_3 \tag{3a}$$

$$\frac{dA_1}{dz} = d_{eff} i \frac{2k_1}{n_o(\lambda_1)} A_2^* A_3 \tag{3b}$$

$$\frac{dA_1}{dz} = d_{eff} i \frac{2k_1}{n_o(\lambda_1)} A_2^* A_3 \tag{3c}$$

Under simplifying assumptions, A_3 can be solved for and it is revealed that the amplitude of the generated field is maximized when $\Delta k = 0$. This is known as the phase-matching condition and is difficult to achieve due to normal dispersion effects in real-world materials. A uniaxial, birefringent nonlinear crystal was used in the simulation to counter these normal dispersion effects. The SFG simulation used these differential equations, along with nonlinear crystal parameters, to propagate the fields through a simulated nonlinear crystal and generate a shaped SFG output pulse.

II. METHODS

A. Input Processing

Previous versions of the simulation used a flat-phase gaussian pulse input with a fixed vector length and sampling rate.[2] The intensity envelope of this parent pulse was generated at the beginning of the simulation using standard optical equations for a flat-phase gaussian and manually-set parameters, such as pulse width, central frequency, and pulse energy. As a result, the pulse type was limited to standard, flat-phase gaussian pulses. In this work, the SFG program was modified so that a more complex pulse, previously shaped using an AOPDF simulator, could be taken as the input. Fig. 2 depicts the modified input processing of the new pulse type prior to the stretching/compressing steps and SFG simulation.

The new type of simulated input pulse was defined by an electric field time profile vector, central wavelength, time vector, and frequency vector which together preserved amplitude, phase, sampling rate, and timescale information. In order to preserve parent pulse phase information, an oscillatory electric field input pulse was used compared to the intensity envelopes employed in previous iterations of the SFG program (Fig. 2a).[2]

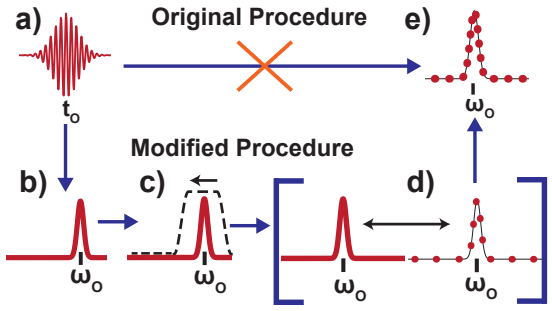

FIG. 2. a) The real component of a gaussian pulse's amplitude in the time domain. b) The real component of a gaussian pulse's amplitude in the frequency domain centered on the central frequency. c) The application of a Tukey filter to the pulse prior to the rotation of its indices with the central frequency being preserved. d) A diagram showing the discrete nature of the pulse prior to interpolation. e) The gaussian pulse in the frequency domain post-interpolation.

For these simulations, the input pulse was taken to have a central wavelength of 1030 nm. The input electric field was transformed into the frequency domain using python's Fast Fourier Transform (FFT) algorithm, yielding a transformed pulse positioned at the central frequency (Fig. 2b). An additional filtering step was introduced whereby either a Hanning or Tukey window filter was applied to the pulse prior to a rotation of indices which re-centered the pulse at the midpoint of the discrete vector while preserving central frequency position (Fig. 2c). The filter was necessary to prevent discontinuities post-rotation which would have hobbled any and all Fourier transforms. The index rotation was necessary to allow the new input pulse-type to be compatible with the original structure of the SFG simulation.

As can be seen in Fig. 2d, the input electric field was a discrete vector with a sampling rate and vector length characteristic to the AOPDF simulation. However, the AOPDF simulation required complete resolution of the electric field oscillations and thus required exceedingly high temporal resolution. This input format was incompatible with the SFG program due to the Fourier split step nature of its pulse propagation. Consequently, an interpolation step was introduced which sacrificed resolution in the time domain and improved resolution in the frequency domain, yielding a vector with a length of 2^{15} and a time resolution of 16.5 fs (Fig. 2e). The linear interpolation was performed separately on the amplitude and phase components of the electric field using a standard python library interpolation function. Following this input processing procedure, the input pulse could then be duplicated and fed into the original stretching/compressing and subsequent SFG simulation stages.

B. Stretching and Compressing

Fig. 3a shows the process by which the processed infrared input pulse was split and each branch given opposite second order dispersion (SOD) and third order dispersion (TOD). The dispersion terms could be manually adjusted for each peak and were introduced via multiplication with the frequency domain pulse shown in Fig. 3e according to Eq. 2. The amplitudes of these two fields, A_1 and A_2, were used as inputs into Eqs. 3a, b, and c in the SFG simulation to generate the output field A_3 (Fig. 3b and c).

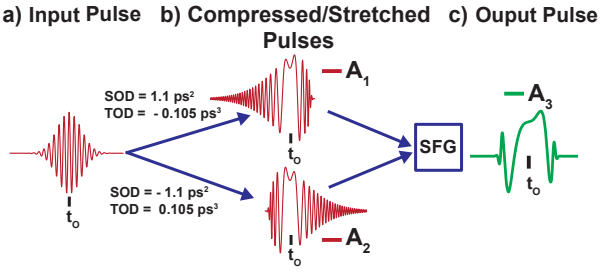

FIG. 3. a) Input pulse electric field in the time domain which is then split into two separate pulses b) Stretched and compressed split pulses with opposite 2nd and 3rd order dispersion values. c) The intensity and real amplitude of the output pulse following SFG simulation.

C. SFG Simulation

When these two oppositely chirped pulses entered the SFG simulation stage, they underwent propagation and frequency mixing in a modeled nonlinear medium. The nonlinear medium was defined by a crystal type, length, and an angle of incidence. The main crystal typed used in the simulations was β–Barium Borate. Additionally, the software was expanded to include a Potassium Dihydrogen Phosphate (KDP) crystal option. The crystal type was used to determine the necessary incidence angle to satisfy the phase matching condition, the effective nonlinear optical coefficients,[4] and the characteristic refractive index constants.[5] The length of crystal through which the electric fields where propagated could be manually adjusted and a value of 2 mm was used for these simulations.

The propagation direction was taken as the z-axis and the crystal divided into a series of 100 steps. Eqs. 3a, b, and c were used in combination with a split-step Fourier method and 4th order Runga-Kutta method to propagate the electric fields through the crystal.[2] Frequency domain calculations processed pulse dispersion and time domain calculations processed nonlinear conversion.[2] Once the electric fields had been fully mixed and propagated through the crystal, the final output pulse was stored for use in later simulations. This stored pulse had a central wavelength of 515 nm and was defined by an electric field time profile vector, central wavelength, time vector, frequency vector, and a list of the SFG simulation parameters. This parameter list included all stretching and compression dispersion terms and relevant nonlinear medium specifications. The next step in the simulation would be to upconvert this 515 nm to a UV pulse.

III. RESULTS AND DISCUSSION

A. Recovery of dispersion shaping

To increase the peak energy of the x-ray pulses produced by the LCLS XFEL, the ideal optical pulse incident on the photocathode was found to possess a near-bullet shape with a flat temporal profile.[6] The ability to modify both pulse duration via an introduced SOD term and the electric field ringing via an introduced TOD term was a key component of the original program as it allowed for the generation of semi-flat temporal pulses.[2] This functionality was recovered following the modification of the pulse input type and processing method. Three sets of pulse pairs and their respective propagated SFG output pulses for a variety of SOD and TOD constants can be seen in Fig. 4. Due to their direct impact on pulse duration and shape, the variation of these SOD and TOD parameters has been predicted to be a critical component in the future machine learning optimization of the LCLS photoinjector system.

B. Preservation of parent pulse phase information

An additional modification to the SFG program was the preservation of parent pulse phase information by enabling the use of oscillating electric field inputs in place of intensity envelopes. The input processing mentioned earlier was crucial to the handling of this oscillating pulse. A comparison of the negatively and positively chirped pulses and their corresponding SFG output pulses with this preserved phase information can be seen in Fig. 5a and b. The plots of the absolute value of the same electric fields squared (intensity plots) can be found in Fig. 5c and d and match those generated from traditional intensity envelope inputs.[2]

The phase information present in the initial pulse incident on the photocathode can be inherited by the electron bunches and hence the resulting x-ray pulses. Enabling this phase information to be propagated through the SFG program and passed on to the photocathode simulator preserves a valuable parameter which can be used in the optimization of the XFEL.

C. Handling phase-shaped parent pulses

The primary motivation behind modifying the pulse input type and processing of the original SFG program was to allow for the input of more exotic pulses, previously shaped by the AOPDF simulator. The modified SFG program was shown to handle input pulses with base levels of first order dispersion, SOD, TOD, and fourth order dispersion. Isolated first order dispersion caused the pulse to shift in its central time. Consequently, the shape of the SFG output was identical to that seen in Fig. 5 for a flat phase gaussian. However, the sole

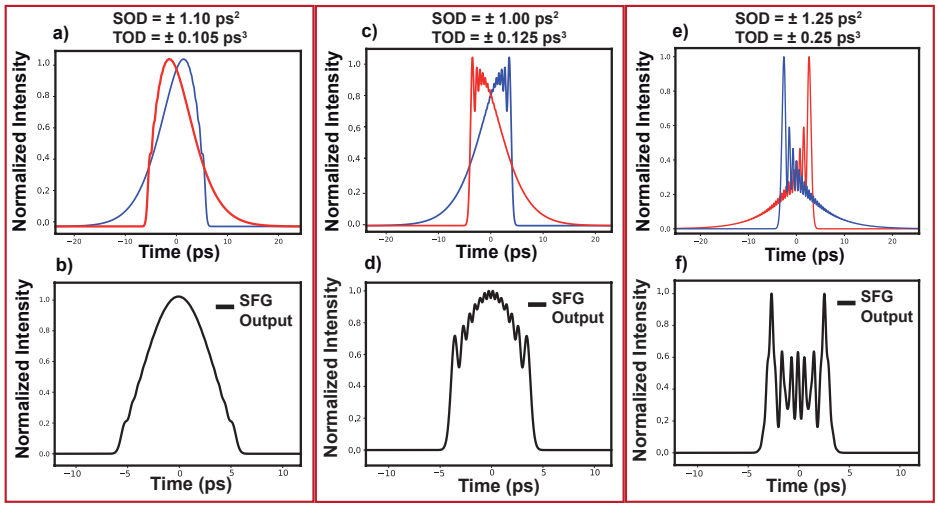

FIG. 4. a), c), and e) The intensity of positively and negatively chirped pulses with added second order dispersion (SOD) and third order dispersion (TOD) in the time domain. The first peak (blue) had positive SOD and negative TOD and the second peak (red) had negative SOD and positive TOD. b), d), and f) Intensity of SFG output electric fields in the time domain.

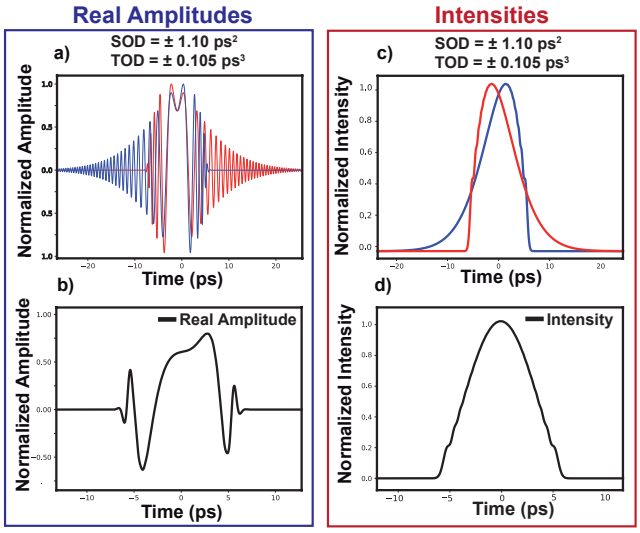

FIG. 5. a) The real amplitude of positively and negatively chirped pulses with preserved phase information. b) The real amplitude of the SFG output with preserved phase information. c) The intensity of positively and negatively chirped pulses with added SOD and TOD. d) The intensity of the SFG output.

SOD, TOD, and fourth order dispersion input peaks resulted in altered chirped input pulses and output SFG pulse, both of which can be seen in Fig. 6.

Fig.6a shows two chirped pulses which were derived from introducing ±1.10 ps^2 SOD and ±0.105 ps^3 TOD to pulses possessing some base level of SOD. Consequently, the broader peak (red) had a net sum of SOD which was larger than that seen in the narrower peak (blue) and these mixed to yield an asymmetric output intensity envelope (Fig. 6b). Fig. 6c shows the same chirping effect but for an input peak possessing a base level of TOD, resulting in the narrower peak (red) having a larger net degree of TOD than the broader peak (blue) and a similarly asymmetric output pulse (Fig. 6d). Lastly, Fig. 6e and f depict two chirped pulses with added fourth order dispersion and the resulting SFG output.

D. Handling amplitude-shaped pulses

The modified SFG program was also demonstrated to handle input peaks which had undergone amplitude shaping by the AOPDF simulator. Fig. 7a shows a flat phase input gaussian pulse with no amplitude shaping in the wavelength domain and Fig. 7b shows the resulting SFG output with its characteristic ringing. For comparison, Fig. 7c depicts a flat phase gaussian with a 5 nm hole at its central wavelength (1030 nm). The resulting SFG output seen in Fig. 7d shows a depressed intensity near the central wavelength which is realistic given the amplitude shaping of the parent, input pulse.

Amplitude shaping via the creation of holes at higher and lower wavelengths relative to the central wavelength was also observed to narrow the pulse timed duration. Consequently, in addition to optimizing the generation of flat time profile peaks, amplitude shaping may have relevant applications in the generation of near-attosecond pulses with increasingly narrow pulse durations.

IV. CONCLUSION

In conclusion, an SFG simulation program was successfully modified to allow for the input of exotic pulses shaped using an AOPDF simulator. The SFG program was additionally modified to preserve parent pulse phase information and allow

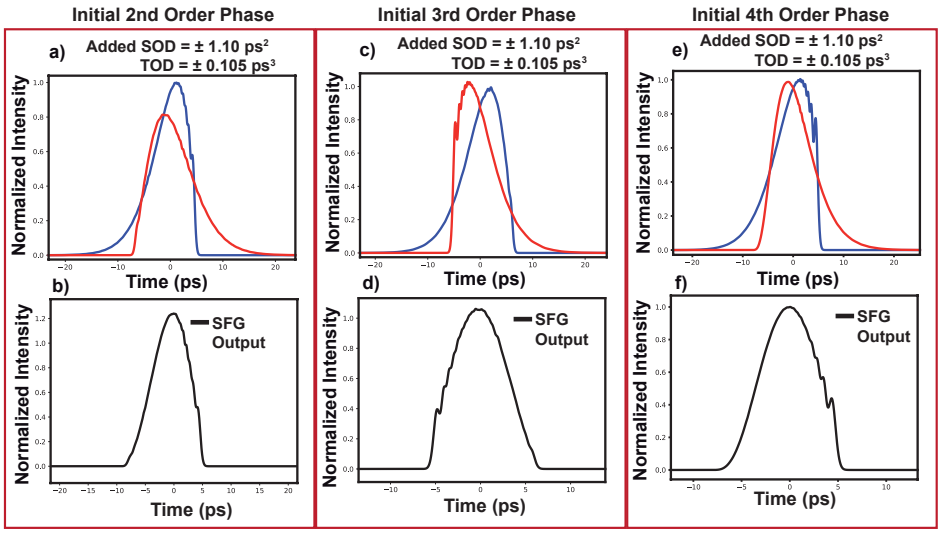

FIG. 6. The intensities of positively and negatively chirped pulses for 2nd order (a), 3rd order (b), and 4th order (e) shaped input peaks with added SOD and TOD dispersion. The intensities of SFG output electric fields for initial input peaks with 2nd order (b), 3rd order (d), and 4th order (f) phase shaping.

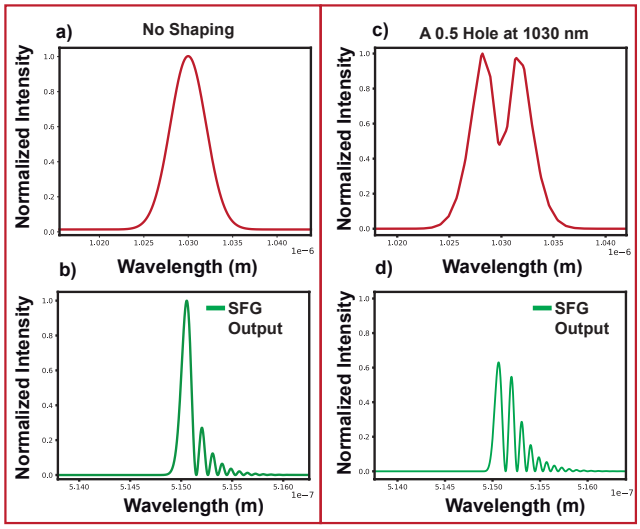

FIG. 7. a) A gaussian input peak in the wavelength domain with no amplitude shaping. b) A gaussian input peak with a 5 nm hole at 1030 nm in the wavelength domain. c) The SFG output pulse for a gaussian input pulse with no shaping. d) The SFG output pulse for an input gaussian pulse with a 5 nm hole at 1030 nm.

for the use of a KDP crystal as the system's nonlinear medium. The modified program was demonstrated to produce physically sensible outputs for both phase- and amplitude-shaped pulses. This was a critical step in the integration of the SFG program into the multi-process simulation of the LCLS XFEL at SLAC and the broader goal of optimizing x-ray pulse generation using machine learning. An important next step will be to use these integrated models to generate data for the machine learning components and to inform the hardware development of the adaptable shaping for the photoinjector laser.

ACKNOWLEDGMENTS

This work was supported in part by the U.S. Department of Energy, Office of Science, Office of Workforce Development for Teachers and Scientists (WDTS) under the Science Undergraduate Laboratory Internships (SULI) program. The author would also like to acknowledge Jack Hirschman and Randy Lemons for providing the original code and advice along with Dr. Sergio Carbajo for his guidance and direction. Lastly, the presenter would like to thank Melina Endsley, Rose Knight, and Shea Charkowsky for their helpful peer review and insight.

[1] C. Bostedt, S. Boutet, D. M. Fritz, Z. Huang, H. J. Lee, H. T. Lemke, A. Robert, W. F. Schlotter, J. J. Turner, and G. J. Williams, "Linac Coherent Light Source: The first five years," Reviews of Modern Physics **88**, 015007 (2016).

[2] R. Lemons, N. Neveu, J. Duris, A. Marinelli, C. Durfee, and S. Carbajo, "Dispersion-controlled Temporal Shaping of Picosecond Pulses via Noncolinear Sum Frequency Generation," (2020), 10.1364/ao.XX.XXXXXX, arXiv:2012.00957v1.

[3] R. W. Boyd, *Nonlinear Optics*, 3rd ed. (Academic Press, San Diego, 2008).

[4] L. Zhu, X. Zhang, M. Xu, B. Liu, S. Ji, L. Zhang, H. Zhou, F. Liu, Z. Wang, and X. Sun, "Refractive indices in the whole transmission range of partially deuterated KDP crystals," AIP Advances **3**, 112114 (2013).

[5] R. C. Eckardt, H. Masuda, Y. X. Fan, and R. L. Byer, "Absolute and Relative Nonlinear Optical Coefficients of KDP, KD*P, BaB2O4, LiIO3, MgO:LiNbO3, and KTP Measured by Phase-Matched Second-Harmonic Generation," IEEE Journal of Quantum Electronics **26**, 922–933 (1990).

[6] D. H. Dowell, "Sources of Emittance in RF Photocathode Injectors: Intrinsic emittance, space charge forces due to non-uniformities, RF and solenoid effects," (2016), arXiv:1610.01242.